Vol. 21, No. 3(2022) Fen2849
Revista Mexicana de Ingeniería Química

A hydrodynamic model to describe $CaCO_3$ deposit formation in pipelines

Modelo cinético hidrodinámico para el estudio de la formación de depósitos de $CaCO_3$ en tuberías

H. Gómez-Yáñez[1]*, G.T. Lapidus-Lavine[2]

[1]*División de Estudios de Posgrado, Facultad de Ingeniería, Universidad Nacional Autónoma de México, Avenida Universidad 3000, Alcadia de Coyoacán, 04510, Ciudad de México, México.*
[2]*Departamento de Ingeniería de Procesos e Hidráulica, Universidad Autónoma Metropolitana-Iztapalapa. Avenida Ferrocarril San Rafael Atlixco número 186, Colonia Leyes de Reforma 1_a sección Alcaldía de Iztapalapa, Ciudad de México, 09310 México.*

Received: June 12, 2022; Accepted: August 1, 2022

Abstract

Calcium carbonate deposition inside of pipes is a widespread problem in aqueous fluid transport systems, where calcium and carbonate ions are dissolved. The present study describes the physical and chemical phenomena of mass transport of the chemical species, from the bulk solution to the pipe walls, inside a straight circular pipe. The mass transfer coefficient is estimated using correlations for developing laminar flow. The controlling mechanism is assigned using the Damköhler number and the model simulation results are analyzed for three scenarios: when mass transfer controls the deposition, by mixed control or by the deposition kinetics. If mass transfer is the controlling mechanism, the deposit was concentrated at the pipe entrance; reflecting the findings in the oil fields, while with kinetic control, it forms further downstream. This study over a straight pipe, found that most important factor influencing the deposition process is the bulk and superficial pH values.
Keywords: calcium carbonate scaling, mass transfer, chemical speciation.

Resumen

La formación de depósitos de carbonato de calcio, al interior de tuberías es un problema generalizado en los sistemas de transporte de fluidos acuosos, donde se disuelven los iones de calcio y carbonato. El presente trabajo describe los fenómenos físicos y químicos del transporte masivo de las especies químicas, desde el seno de la solución hasta las paredes de la tubería, dentro de una tubería circular recta. El coeficiente de transferencia de masa se estimó utilizando correlaciones para flujo laminar en desarrollo. El mecanismo de control se determinó por medio del número de Damköhler, y los resultados de la simulación del modelo se analizaron para tres escenarios: control por transferencia de masa, control mixto y control por cinética en la formación del depósito. Cuando la transferencia de masa es el mecanismo de control, el depósito se concentró en la entrada de la tubería; confirmando lo observado en los campos petroleros, mientras que, con control cinético, se formó a una distancia aguas abajo. En este estudio se encontró que el factor más importante que influye en el proceso de formación de depósito es el valor del pH en el seno del fluido, y el pH sobre la superficie de contacto.
Palabras clave: depósitos de carbonato de calcio, incrustaciones, transferencia de masa, especiación química.

*Corresponding author. *E-mail*: gomez.hector@colpos.mx
https://doi.org/10.24275/rmiq/Fen2849
ISSN:1665-2738, *issn-e*: 2395-8472

1 Introduction

Chemical Engineering is a discipline that covers a wide range of applications, for which it relies mainly on Transport Phenomena; for the solution of problems such as mineral deposits present in the oil industry. When petroleum reservoirs reach a mature stage, water accompanies the extraction of the hydrocarbons. Once the water is separated, it is recirculated back through injection wells; the procedure is commonly known as secondary oil recovery (Lake, 1989, Bailey *et al*., 2000, Kang *et al*., 2018; Zhang *et al*.; 2018). However, this aqueous phase contains elevated concentrations of dissolved ions, especially calcium and carbonate (Rostron, 2018). As the fluid flows through the petroleum production system, the chemical equilibria in the solution may change with the ambient conditions, causing precipitation and mineral deposit formation or scaling.

The mineral deposits or scale is the accumulation of material that can lead to blockage and prevented the fluid flow in the well bore, production pipes, valves, casing, and downhole equipment (Kammal *et al*., 2018). These deposits obstruct the flow by reducing the pipe radius, a condition that worsens with time (SPE, 2017). The formation of calcium carbonate deposits occurs in hydrocarbon collection systems (oil with water).

Mainly, the problem arises at points where there is flow direction changes or at the pipe entrance, where developing flow profiles occur. In these areas, calcium carbonate deposits are common, such as those shown in Figure 1 in an elbow of a surface gathering system in an oil field in western Texas. In this case, the deposit originated at points where there is a change in the flow pattern, (Cowan & Weintritt, 1976). In this study, only chemical phenomena in the developing boundary layer at pipe entrances are considered; despite this limitation, the principles presented may be applied to other geometric changes employing the corresponding mass transfer coefficients for the particular situation.

In the oil industry, sites have been identified that are conducive to the development of mineral deposits. Figure 2 outlines the locations where the problem of mineral deposit formation is present (Crabtree *et al*., 1999):

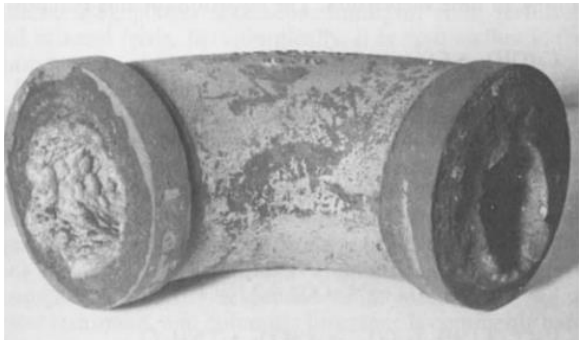

Fig. 1. Scale formation at the elbow inlet, (Cowan & Weintritt, 1976).

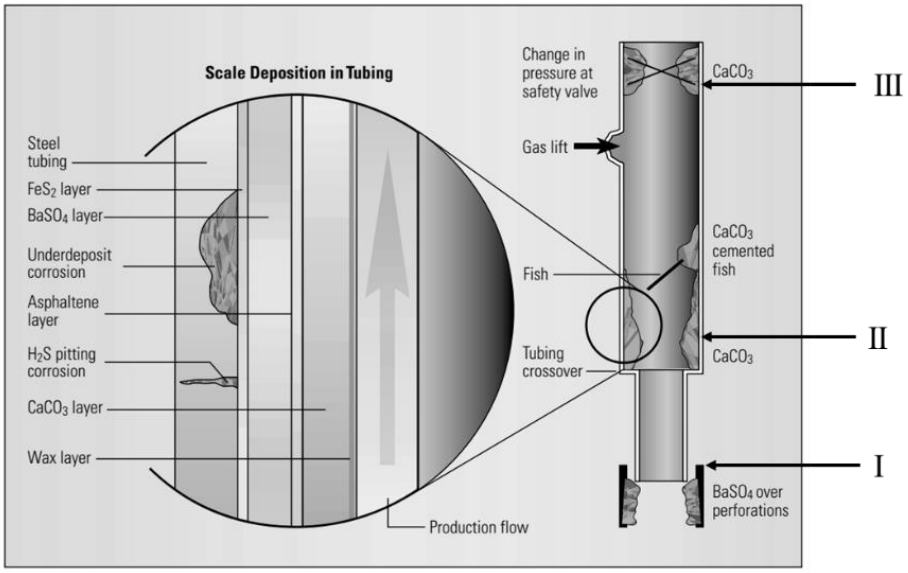

Fig. 2. Location of scale deposits in tubing, (Crabtree *et al*., 1999).

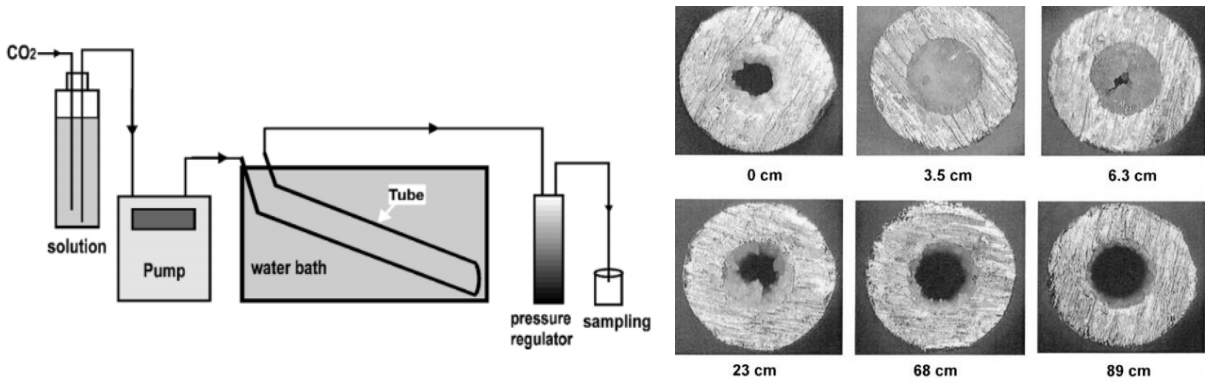

Fig. 3.a) Experimental equipment disposition, 3.b) Scale deposition profiles, (Zhang *et al*., 2001).

1. well completion (perforated interval),
2. change of geometry of the system, causing a recirculation of the fluid,
3. chokes, valves, and pipefittings where high-pressure drops occur.

Location I) corresponds to the entrance of a straight pipe, which is the subject of this research.

Experimental research of pipe blockage and the investigation into the effects of changing flow regimens have been undertaken; however, theoretical analyses focused on explaining experimental findings are uncommon. One of these studies is shown in Figure 3, where the schematic of an experimental set-up is displayed (see Fig. 3.a). The experimental system consists of a 1m long steel pipe; at the exit, the concentrations of calcium ions and alkalinity are monitored. The results of the study show clogging (see Fig. 3.b) caused by calcium carbonate deposit formation at lengths of the tube that approximately coincide with changes in flow direction (Zhang *et al*., 2001).

Although these occurrences are documented in the literature, there have been very few attempts to describe this phenomenon from the standpoint of chemical equilibria. Some of them, authored by Weichers *et al*., (1975), Eroni *et al*., (2013); Zhu *et al*., (2015), studied the nucleation kinetics in a supersaturated solution of calcium and carbonate ions, seeded with solid particles of the same material; the authors performed a speciation analysis of the solution and related the kinetics to the degree of supersaturation. Furthermore, the results indicate that spontaneous precipitation in solution is not favored, rather the precipitation exclusively on the seeds (solid surfaces). Despite the insight provided by this investigation, the teachings have not been applied to a flow system.

On the other hand, Chan & Ghassemi (1991 a & b) presented a chemical flow model to describe calcium carbonate fouling in laminar falling films with simulation results that approach experimental data in heat exchangers under some conditions. However, their single-species and multispecies models did not predict deposition velocity based on the local species concentrations nor they did consider the possibility of changing mass transfer coefficients as a function of distance along the pipe or plate surfaces.

More recently, Segev *et al*., (2012) incorporated chemical equilibrium into a fully developed turbulent flow model; nevertheless, for similar reasons, it does not explain the calcium carbonate accumulation in particular locations. For that reason, the purpose of the present study is to formulate a phenomenological flow model, incorporating dynamic chemical equilibria and deposition kinetics, to describe calcium carbonate formation in developing laminar flow. The results of the simulation will explain the preferential deposition in specific areas of the hydraulic system.

2 Description of the physical phenomena

2.1 Chemical speciation

Calcium carbonate scales or deposits are the product of the interaction between calcium and carbonate ions dissolved in a supersaturated solution (see Fig. 4),

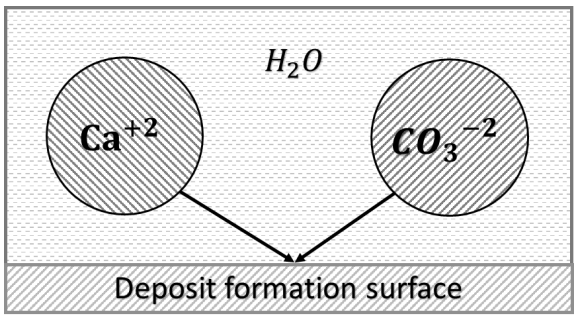

Fig. 4. Calcium and carbonate ions dissolved in liquid phase.

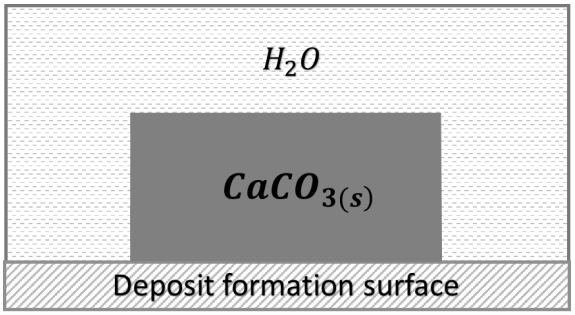

Fig. 5. Formation of the solid calcium carbonate on the surface.

according to the following reaction.

$$CaCO_{3(s)} \leftrightarrow Ca^{2+} + CO_3^{2-},\ \log_{10}(K_{sp}) = -8.48 \quad (1)$$

The solid calcium carbonate deposition preferentially occurs on solid surfaces (see Fig. 5), such as pipe walls.

The model, which is developed below, describes the process of calcium carbonate scaling, generated from supersaturated aqueous solutions containing Ca^{2+} and CO_3^{2-} ions. The dissolved ions in aqueous solution produce many soluble chemical species, which are in equilibrium and may be described by the following chemical reactions (Wiechers *et al.*, 1975; MEDUSA, 2010):

$$2H^+ + CO_3^{2-} \leftrightarrow H_2CO_3^0,\ \log_{10}(K_2) = 16.681 \quad (2)$$

$$H^+ + CO_3^{2-} \leftrightarrow HCO_3^-,\ \log_{10}(K_3) = 10.392 \quad (3)$$

$$H_2O \rightarrow H^+ + OH^-,\ \log_{10}(K_4) = -14.000 \quad (4)$$

$$Ca^{2+} + CO_3^{2-} \leftrightarrow CaCO_3^0,\ \log_{10}(K_5) = 3.224 \quad (5)$$

$$Ca^{2+} + H^+ + CO_3^2 \leftrightarrow CaHCO_3^+,\ \log_{10}(K_6) = 11.435 \quad (6)$$

$$H_20 + Ca^{2+} \leftrightarrow H^+ + CaOH^+,\ \log_{10}(K_7) = -12.780 \quad (7)$$

The numerical value of each equilibrium constant was obtained from the HYDRA database at 25°C, (MEDUSA, 2010). Although the total carbonate ion concentration in the aqueous solution is a result of the absorption of gaseous carbon dioxide, $CO_{2(g)}$, this equilibrium is not included in the present model (constant pressure).

It is important to note that the above equilibrium constants were reported considering the concentrations in molarity [mol L^{-1}]. For insertion into the transport model, the concentrations and corresponding equilibrium constants were converted to [mol m^{-3}] to ensure unit consistency.

To account for the dynamic equilibria between the chemical species appearing in reactions (2)-(7), these will be grouped as the concentration of total functional groups and the corresponding transport equations will be developed in terms of these total chemical species (Wiechers *et al.*, 1975; Lapidus, 1992). In this case, three total groups are involved:

Calcium species or total calcium:

$$[Ca_T] = [Ca^{2+}] + [CaOH^+] + [CaHCO_3^+] + [CaCO_3^0], \quad (8)$$

Carbonic species or total carbonate:

$$[C_T] = [CO_3^{2-}] + [HCO_3^-] + [H_2CO_3^0] + [CaCO_3^0] + [CaHCO_3^+], \quad (9)$$

Hydrogen species or total hydrogen (not including water):

$$[H_T] = [H^+] + [HCO_3^-] + [CaHCO_3^+] + 2[H_2CO_3^0], \quad (10)$$

The concentrations of individual chemical species are determined by the equilibrium constants of reactions (2)-(7) at any point in the flow system.

2.2 *Saturation ratio*

Once the chemical speciation is known, given the pH, $[Ca_T]$ and $[C_T]$, the next step is the calculation of the degree of supersaturation in the system; this characterization is known as the saturation ratio, SR. The saturation ratio is the thermodynamic parameter, which indicates if the formation of a solid phase is possible (see Table 1).

The saturation ratio is function of the thermodynamic activity of the ions that produce the calcium carbonate free (uncomplexed), calcium and

carbonate ions, and its solubility product (Zhang & Dawe, 1997):

$$SR = \frac{a_{Ca^{2+}} * a_{CO_3^{2-}}}{K_{sp}} \tag{11}$$

Ionic activities are described by:

$$a_{Ca^{2+}} = f_{Ca^{2+}} * [Ca^{2+}], \tag{12}$$

$$a_(CO_3^{2-}) = f_{CO_3^{2-}} * [CO_3^{2-}], \tag{13}$$

In this development, the effect of the change in ionic strength of the solution on the activity coefficients and the value of the solubility product has been assumed negligible, although a rigorous analysis should include this factor.

Considering the previous simplification, the activities can be approximately by the concentrations:

$$a_{Ca^{2+}} \approx [Ca^{2+}], \tag{14}$$

$$a_{CO_3^{2-}} \approx [CO_3^{2-}], \tag{15}$$

Substituting these into the saturation ratio definition (11):

$$SR = \frac{[Ca^{2+}] * [CO_3^{2-}]}{K_{sp}}, \tag{16}$$

Therefore, calcium carbonate scaling is possible only when the solution is supersaturated, SR>1.

2.3 *Mass transfer from bulk solution to interface*

The driving force for calcium carbonate deposition is the chemical species concentration difference between that in the bulk solution and at the liquid - solid interface. In a flow system, the mass transfer process occurs within a thin fluid layer next to pipe wall with a variable velocity profile; the thickness of this boundary layer will be referred to as δ_c (Lobo-Oehmichen, 2007).

The mass transfer in scale formation process involves two boundaries (see Fig. 6):

1. in the bulk solution (∞), which is assumed homogeneous.
2. at the liquid-solid interface (i).

The chemical species distribution, which was described in (2) - (7), is valid at both boundaries.

In the bulk solution, (∞):

a) Calcium species or total calcium:

$$[Ca_T]_\infty = [Ca^{2+}]_\infty + [CaOH^+]_\infty + [CaHCO_3^+]_\infty + [CaCO_3^0]_\infty \tag{17}$$

b) Carbonic species or total carbonate:

$$[C_T]_\infty = [CO_3^{2-}]_\infty + [HCO_3^-]_\infty + [H_2CO_3^0]_\infty + [CaCO_3^0]_\infty + [CaHCO_3^+]_\infty, \tag{18}$$

c) Hydrogen species or total hydrogen:

$$[H_T]_\infty = [H^+]_\infty + [HCO_3^-]_\infty + [CaHCO_3^+]_\infty + 2[H_2CO_3^0]_\infty, \tag{19}$$

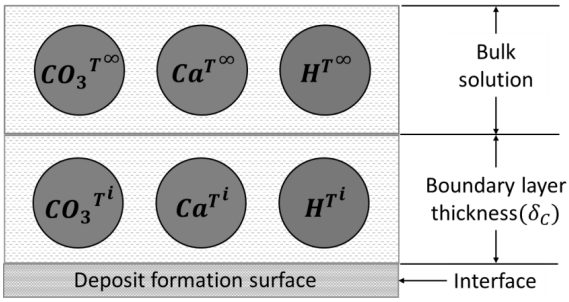

Fig. 6. Bulk solution and interface concentrations.

Table 1. Classification of the solution.

Unsaturated solution	Saturated solution	Supersaturated solution
SR<1 $\log(SR) < 10$ The solution has the capacity to dissolve more salts (more ionic content is accepted by the solution) before reaching saturation.	SR=1 $\log(SR) = 0$ The solution is in chemical equilibrium. The solid phase is not present.	SR>1 $\log(SR) > 10$ The solution is thermodynamically unstable and has the capacity to form solids.

Therefore, bulk phase saturation ratio may be expressed as:

$$SR_{\infty} = \frac{[Ca^{2+}]_{\infty} * [CO_3^{2-}]_{\infty}}{K_{sp}} \tag{20}$$

In an analogous manner, for the liquid - solid interface (i):

a) Calcium species or total calcium:

$$[Ca_T]_i = [Ca^{2+}]_i + [CaOH^+]_i + [CaHCO_3^+]_i + [CaCO_3^0]_i, \tag{21}$$

b) Carbonic species or total carbonate:

$$[C_T]_i = [CO_3^{2-}]_i + [HCO_3^-]_i + [H_2CO_3^0]_i [CaCO_3^0]_i + [CaHCO_3^+]_i, \tag{22}$$

c) Hydrogenic species or total hydrogen:

$$[H_T]_i = [H^+]_i + [HCO_3^-]_i + [CaHCO_3^+]_i + 2[H_2CO_3^0]_i, \tag{23}$$

Therefore, the liquid-solid interface (surface) saturation ratio may be calculated using the following expression:

$$SR_i = \frac{[Ca^{2+}]_i * [CO_3^{2-}]_i}{K_{sp}}, \tag{24}$$

The mass transfer process, per unit area, is described by the mass flux of total calcium and total carbonate that take place from the bulk solution to the pipe wall.

2.4 Mass transfer coefficient model

In the present model, the bulk solution is assumed homogeneous both in velocity, as well as in concentration at the pipe inlet; this condition can also be applied to the fluid after an abrupt reduction, ampliation or directional change in the pipe. Under these conditions, and in laminar flow, the fluid has not yet reached a completely developed velocity profile and mass transfer takes place through the boundary layer; in turn, this has a variable width (δ_c) as a function of the distance from the pipe inlet (Lobo-Oehmichen, 2007). Since the velocity profile and the boundary layer characteristics are changing with both the radial and longitudinal coordinates, mass transfer of the soluble species between the bulk solution and the interface is commonly described by the driving force (SR in this case) and local mass transfer coefficients, k_m, which is estimated with empirical correlations as a function of the Reynolds number, Re, and the distance from the pipe inlet (see Eq. (34)).

$$\begin{pmatrix} \text{Molar flux of total} \\ \text{calcium or carbonate} \\ \text{per unit of time} \\ \text{and wetted area)} \end{pmatrix} = k_m \Big(\text{ driving force } \Big) \tag{25}$$

Total calcium flux:

$$N_{Ca_T} = k_m * ([Ca_T]_{\infty} - [Ca_T]_i), \tag{26}$$

Total, carbonate flux:

$$N_{C_T} = k_m * ([C_T]_{\infty} - [C_T]_i), \tag{27}$$

The total calcium flux (N_{Ca_T}) and total carbonate flux (N_{C_T}) have the same direction, toward the deposit formation surface or pipe wall surface (see Fig. 7).

According to the stoichiometric relationship in (1), both fluxes (total calcium and total carbonate) are equal.

$$N_{Ca_T} = N_{C_T}, \tag{28}$$

Considering that the mass transfer coefficients are primarily a function of the flow velocity and the fluid properties, expressed as Re, and that the diffusivities of the different soluble species are of the same order of magnitude, their mass transfer coefficients can be deemed very similar. Expressing the total fluxes as functions of the difference between the concentrations in the bulk and at the interface, (28) is simplified as follows:

$$([Ca_T]_{\infty} - [Ca_T]_i) = ([C_T]_{\infty} - [C_T]_i), \tag{29}$$

In the case of the total hydrogen flux, this is equal to zero because the deposit formation of calcium carbonate does not involve the net consumption or generation of hydrogen:

$$N_{H_T} = 0, \tag{30}$$

Substituting the total hydrogen in terms of flux relation:

$$k_m * ([H_T]_{\infty} - [H_T]_i) = 0, \tag{31}$$

Hence:

$$[H_T]_{\infty} = [H_T]_i, \tag{32}$$

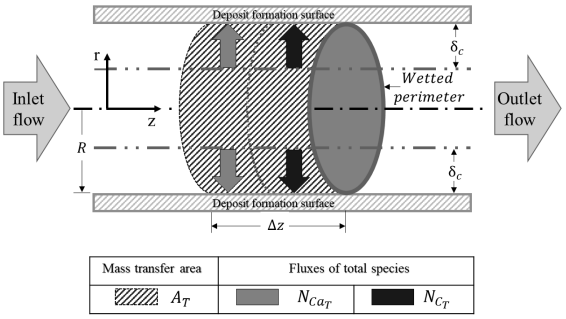

Fig. 7. Mass transfer process towards the pipe surface.

3 Mass transfer coefficient

For the estimation of the mass transfer coefficient, correlations for a straight pipe, the velocity and concentration boundary layer theory for developing flow are employed; these describe the following phenomena:

Velocity Boundary layer.

Zone 1) below the boundary layer, shear stress is caused by the non-slip condition over the surface.

Zone 2) above boundary layer, the fluid is not affected by the shear stress.

Concentration Boundary Layer

Zone 1) below the concentration boundary layer, the concentration at interface depends on the kinetics of the precipitation reaction.

Zone 2) above the concentration boundary layer, the concentration is that of the bulk solution.

Each theory involves the thickness of the boundary layer: for velocity, the boundary layer thickness is represented by δ and the concentration boundary layer thickness is δ_c In both cases (see Fig. 8), the thickness is a function of the distance from the pipe inlet. The correlations are based on the theoretical solution of the fluid and mass transport equations; both are evaluated in each zone of the two boundary layers (Skelland, 1974).

By definition, the Sherwood number (Sh) involves the transport and mass transfer processes (Cussler, 2009):

$$Sh_j = \frac{k_m * d}{\mathscr{D}} \tag{33}$$

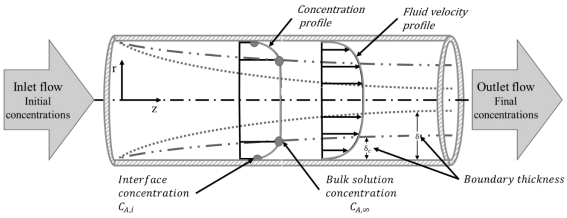

Fig. 8. Velocity and concentration boundary layers.

For cylindrical straight pipe, laminar and developing flow, the expression for local Sherwood number is presented in function of Reynolds and Schmidt number, taken from Skelland´s book (1974), and derived by Lévêque (1928):

$$Sh_j = 1.62 * \left(\frac{d_t}{L}\right)^{1/3} * (Re * Sc)^{1/3} \tag{34}$$

The mass transfer coefficient is an inverse function of the concentration boundary layer thickness, (δ_C). In general, as the thickness of the boundary layer increases (with distance from the inlet), mass transfer is slower.

3.1 Boundary conditions: saturation ratio at the solid-liquid interface

As was mentioned previously, calcium carbonate precipitation requires a saturation ratio greater than unity:

$$SR_i > 1, \tag{35}$$

Calcium carbonate scale is assumed only to form on the wall surface.

The boundary condition at the solid-liquid interface (inner pipe radius) is the local saturation ratio. At this boundary, the formation of the calcium carbonate scale occurs:

$$SR|_{r=R} = SR_i, \tag{36}$$

On the pipe wall, the interfacial saturation ratio (see Fig. 9) for a discrete distance from the fluid inlet.

At the surface ($r = R$), the total calcium and carbonate flux or global flux, N_G, is equal to the velocity of the precipitation reaction, $\mathbb{R}_{CaCO_3}$:

$$N_{Ca_T} = N_{C_T} = N_G = \mathbb{R}_{CaCO_3}, \tag{37}$$

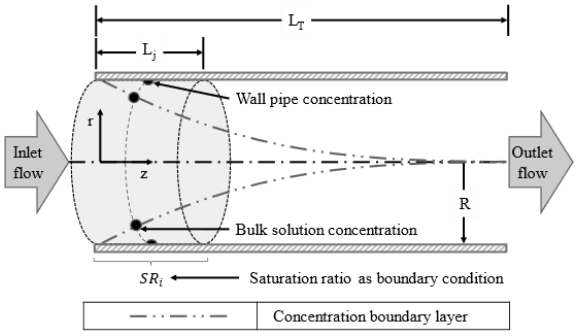

Fig. 9. Saturation ratio as boundary condition.

The calcium carbonate precipitation kinetics are dictated by many factors, including the ratio of the free calcium and carbonate ions concentrations at the interface and the solubility product (Wiechers *et al.*, 1975; Wolthers *et al.*, 2012), as well as the effective wetted pipe surface area, a.

$$R_{CaCO_3} = k_c * K_{sp} * (SR_i - 1) * a \tag{38}$$

where, $(SR_i - 1)$ can be considered the driving force for the reaction.

This last parameter (a), is a function of the rugosity of the pipe wall material ($a = 1$, for smooth material).

$$a = \frac{\text{Available scale area}}{\text{Pipe wall area}}, \tag{39}$$

Equation (38) is an unconventional manner to describe kinetics; however, it implies that the precipitation rate may be considered a linear function of the local Saturation Ratio. The units of k_c are therefore mol/(m^2 s) [m^3/mol]^2, since the Saturation Ratio and "a" are dimensionless. Therefore, to calculate the Damköhler number, k'_m should have the same units. Furthermore, mass flux is a linearly driven phenomenon. Therefore, to develop an equivalence to solve equation (37), $(SR_\infty - SR_i)$ was adapted as the driving force for mass transfer and the corresponding relation for N_G as follows.

$$N_G = k'_m * K_{sp} * (SR_\infty - SR_i) \tag{40}$$

Combining equations (38) and (40):

$$k'_m * (SR_\infty - SR_i) = k_c * (SR_i - 1) * a \tag{41}$$

At this point, the Damköhler number may be introduced; it denotes the relative importance of the chemical reaction (scaling) kinetics with respect to the mass transfer rate and is indicative of the rate-controlling step of the scaling process.

$$Da_{II} = \frac{\text{Chemical reaction kinetics rate constant} \cdot a}{\text{Mass trasfer rate constant}}, \tag{42}$$

$$Da_{II} = \frac{k_C * a}{K'_M}, \tag{43}$$

Substituting this definition into (41) and solving for SR_i:

$$(SR_\infty - SR_i) = Da_{II} * (SR_i - 1), \tag{44}$$

$$SR_i = \frac{(SR_\infty + Da_{II})}{(1 + Da_{II})}, \tag{45}$$

Therefore, the surface saturation ratio SR_i is a function of the controlling mechanism. With very large Damköhler numbers, the deposit formation reaction is fast, and the mass transfer is the slower process or controlling process; in this case, the value of SR_i tends to 1. On the contrary, when the Damköhler number is low (slow reaction), SR_i approaches the saturation ratio of the bulk solution, SR_∞.

4 Solution of the mathematical model

In this section, the methodology used to solve the system of equations that describes the calcium carbonate scale formation phenomena as a function of the distance from the pipe inlet, is presented.

4.1 Determination of the saturation ratio

Firstly, the chemical speciation of the calcium and carbonate ions in the bulk solution is established. The model uses three inlet parameters: bulk solution pH, total calcium ion and total carbonate ion concentrations. The system of equations, (2) - (7) and (17) - (19) with the inlet parameters, is solved simultaneously to estimate the concentrations of all the soluble species involved. From the calculated values of $[Ca^{2+}]$ and $[CO_3^{2-}]$, the SR_∞ is determined by (20).

Next, the initial Damköhler number, Da_{II0}, is fixed; this step determines the control mechanism, which establishes the value of the boundary condition, (45). Once SR_i is estimated, this value, together with the chemical equilibria (2) - (7), the functional groups in the bulk solution (17) - (19), the relation between the reagent fluxes (29) and the total hydrogen flux (32),

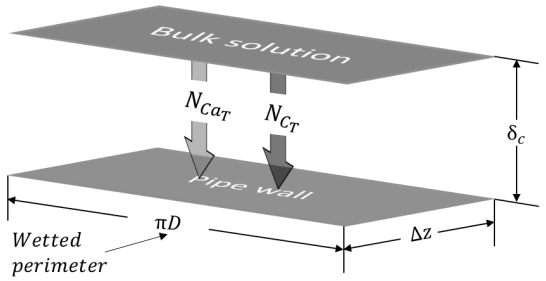

Fig. 10. Transport between the bulk solution to pipe wall surface.

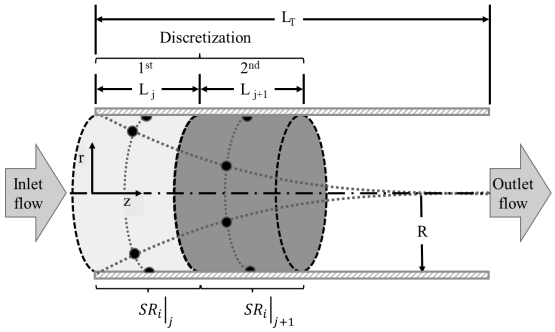

Fig. 11. Second length discretization.

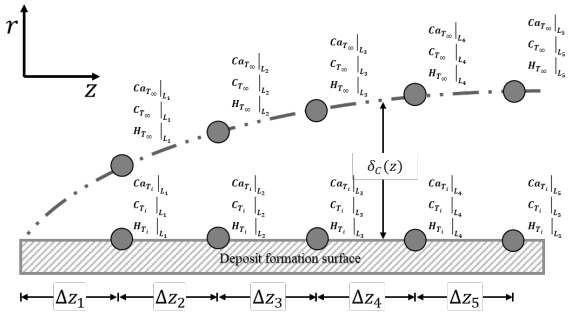

Fig. 12. Illustration of five discrete lengths.

are used to calculate the speciation and the local pH at the solid-liquid interface.

4.2 Mass transfer to the pipe wall

The calcium carbonate deposition only occurs on the pipe wall (surface) (see Fig. 10) and therefore, the kinetics may be represented by a heterogeneous chemical reaction. The reaction area is the product between wetted perimeter and the discretized pipe length:

$$\Delta A_T = \pi * D * \Delta z, \tag{46}$$

The temporal variable may be expressed in terms of the discretized length and velocity of the fluid:

$$t = \Delta t = \frac{\Delta z}{v^0} \tag{47}$$

Substituting into flux equation, the molar flow, mass transfer coefficient, transfer area and time equation:

Total calcium molar flow:

$$\dot{n}_{Ca_{T_{trans}}}\Big|_j = 1.62 * \left(\frac{\pi * \Delta z^2 * \mathscr{D}}{v^0}\right) * \left(\frac{d_t}{L}\right)^{1/3} * (Re * Sc)^{1/3} * ([Ca_T]^{\infty} - [Ca_T]^i) * 10^3, \tag{48}$$

Total carbonate molar flow:

$$\dot{n}_{C_{T_{trans}}}\Big|_j = 1.62 * \left(\frac{\pi * \Delta z^2 * \mathscr{D}}{v^0}\right) * \left(\frac{d_t}{L}\right)^{1/3} * (Re * Sc)^{1/3} \cdot ([C_T]_{\infty} - [C_T]_i) * 10^3, \tag{49}$$

4.3 Mass balance

The mass transfer to the pipe wall, which affects the concentration in the bulk solution, is calculated in discrete sections (Δz), initializing at the pipe entrance (see Fig. 11). Mass balances for total calcium and carbonate are performed and the amount of calcium carbonate precipitated was subtracted from the total amount entering the previous section ($(\pi D^2)/4 * \Delta z * [Ca_T]_{\infty}$ or $(\pi D^2)/4 * \Delta z * [C_T]_{\infty}$), establishing the value of the parameters for the second length segment. The entire procedure is repeated for each subsequent length of pipe, including the recalculation of the Damköhler number (= $f(z)$).

The second discretization calculations give the total concentration for the next section. Figure 12 shows an example of five discretized pipe lengths; each point has three inlet parameters (pH_{∞}, total calcium and carbonate ion concentrations in the bulk solution).

4.4 Mass accumulation over time

Equations (48) and (49), coupled to the Reynolds number, Re, were employed to calculate the deposition for the initial time. Thereafter, the same procedure was used to describe the calcium carbonate deposit accumulation for subsequent times.

$$n_{CaCO_{3_{produced}}}\Big|_j^{t_k} = k * \Delta t * \dot{n}_{C_{T_{trans}}}\Big|_j \tag{50}$$

5 Results and discussion

As was previously mentioned, calcium carbonate deposition involves two sequential steps: first, the reacting species is transported from the bulk solution across the boundary layer to the solid surface (pipe wall). Once at the surface, the chemical species react, producing the solid calcium carbonate. In the following sections, the results of the simulations for the deposition, under distinct controlling mechanisms (mass transfer, kinetics or mixed regime), are discussed. Since the precipitation kinetics depends on, among other properties (Zhang *et al*., 2001, Eroni *et al*., 2013; Zhu *et al*., 2015), the pipe characteristics, such as materials of construction and roughness factor, the analysis will be presented as a function of the controlling (slowest) step in the process. For all cases, the initial pH was 9 and the concentrations of total calcium and carbonate were both 0.0015 M, respectively. The total carbonate concentration and initial pH were employed in accordance with those reported by Weichers *et al*. (1975), to assure a calcium carbonate formation scenario. The total calcium concentration was selected because of the equimolar reaction; however, it represents a common value in industrial applications. For this study, the simulation was terminated at the pipe length corresponding to the transition to fully developed flow for the Reynolds' number employed (Re = 2000), approximately L_e =1250 cm, pipe diameter = 0.1 m and smooth pipe material, a = 1. The pipe diameter selected for the simulation is that which is commonly used in the oil industry (Epelle *et al*., 2018). MATLAB software was employed to solve the system of equations.

5.1 Mass transfer control

In this situation, the mass transfer takes much longer than the calcium carbonate precipitation step. Therefore, the Damköhler number is large; for the simulation, an initial Damköhler equal to 100 was used. The precipitation, SR_∞, SR_i and pH behaviors under this condition, as a function of distance from the pipe inlet, are showed in the following figures (Figures 13.a, 13.b and 13.c). The scaling is greatest near the entrance of the pipe (see Fig 13.a), which may be expected since the concentration boundary layer is at its minimum thickness and the value of k_m assumes its highest value; as a result, Damköhler also increases with distance (see Fig. 13.a), resulting an even greater mass transfer limitation, causing slower precipitation. The resulting calcium carbonate deposit decreases exponentially over the pipe length.

As part of the analysis, Figure 13.b shows the behavior of SR_∞ and SR_i over the pipe length. As mentioned previously, when mass transfer is controlling (fast precipitation kinetics), the interfacial saturation ratio, SR_i (dashed line in Figure 13.b) is approximately unity; this varies only slightly with length, according to equation (45). However, the bulk solution saturation ratio, SR_∞, decreases significantly, even though the bulk solution concentrations of total calcium and carbonate remain almost constant (not shown here because the total concentration changes are negligible). This behavior can be explained by the changes in pH.

As the fluid moves downstream the pipe, its pH tends to become more acid (decrease in pH), this is because even a slight reduction in carbonate and/or calcium concentration (~0.0015 M) affects the $[H^+]$, which is almost 6 orders of magnitude smaller (10^{-9}). At this initial pH, the decrease in carbonate or calcium liberates the hydrogen ion, as can be inferred by reactions (3), (6) and (7). This is also the situation at the solid surface as shown in Figure 13.c, where the pH is more than one unit lower.

Furthermore, the saturation rate tends to decrease as the pH decreases (see Fig. 14), as the speciation diagram indicates. Below the equilibrium line, calcium carbonate precipitation cannot occur if incrustation exists, it will dissolve.

5.2 Mixed control

Mixed control mechanism occurs when the reaction and the mass transfer coefficients are initially of the same magnitude. For this case, an initial Damköhler number of 1 was employed. In this situation, the most important formation of calcium carbonate is still at the inlet of the pipe, but the scale profiles are smaller than the mass transfer controlling mechanism. (See Fig. 15.a). The driving force, represented by the difference between bulk saturation ratio, SR_∞ and interfacial saturation ratio, SR_i, initially has a smaller value compared to the mass transfer case, but remains appreciable further into the pipe length (see Fig 15.b). The pH difference between the bulk solution and the surface, as well as the variation along the tube, are also less substantial.

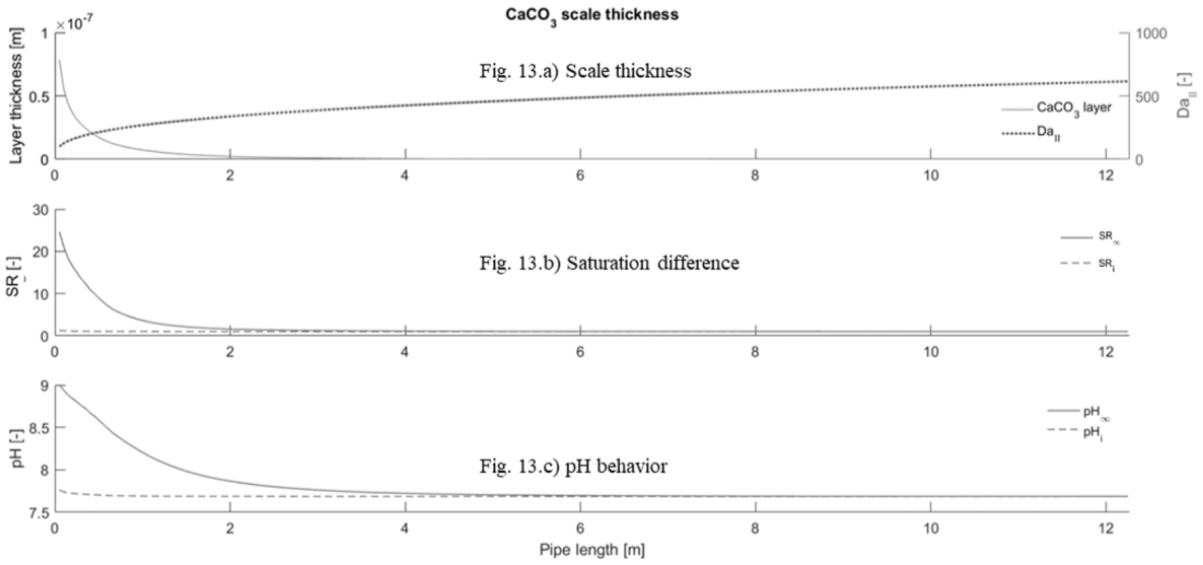

Fig. 13. Mass transfer controlling mechanism simulation results (initial DaII = 100). Initial bulk solution conditions: pH = 9, $[Ca_T]_\infty = [C_T]_\infty$ = 0.0015 M. Flow conditions: Re=2000 & pipe diameter = 0.1 m. t = 40 minutes.

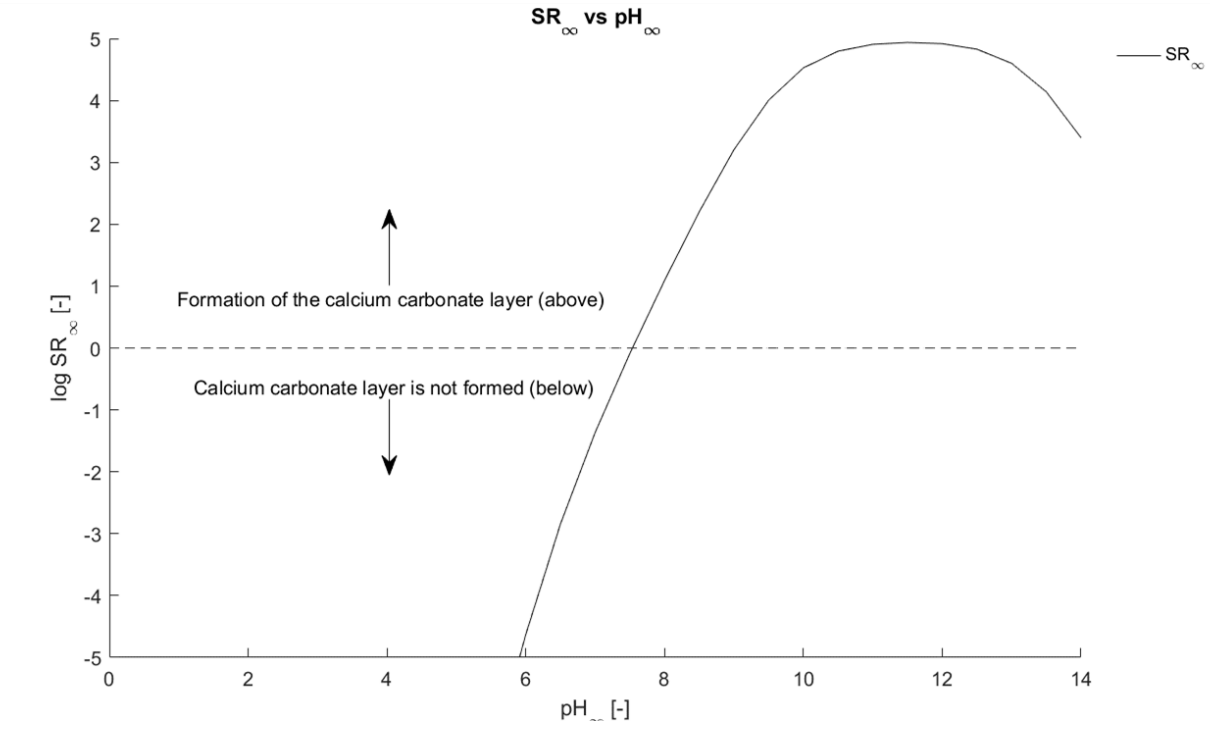

Fig. 14. Layer calcium carbonate scale presence in function of pH. Initial bulk solution conditions: pH = 9, $[Ca_T]_\infty = [C_T]_\infty$ = 0.0015 M. Flow conditions: Re=2000 & pipe diameter = 0.1 m. t = 40 minutes.

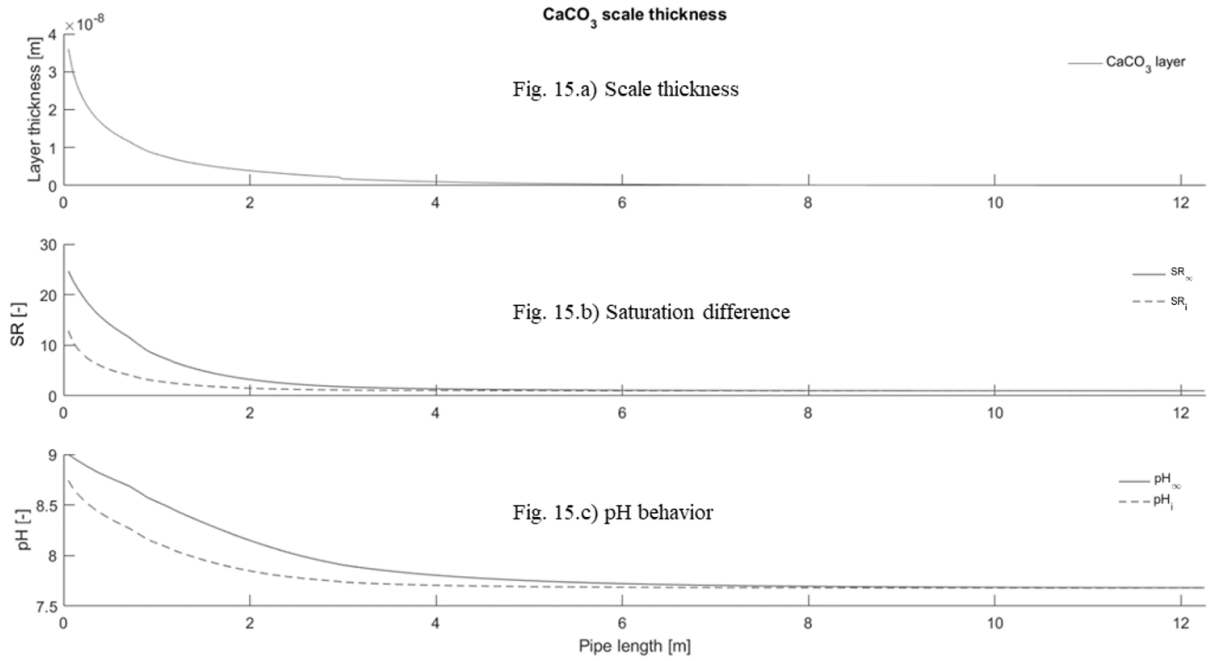

Fig. 15. Mixed control mechanism behavior (initial DaII = 1). Initial bulk solution conditions: pH = 9, $[Ca_T]_\infty$ = $[C_T]_\infty$ = 0.0015 M. Flow conditions: Re=2000 & pipe diameter = 0.1 m. t = 40 minutes.

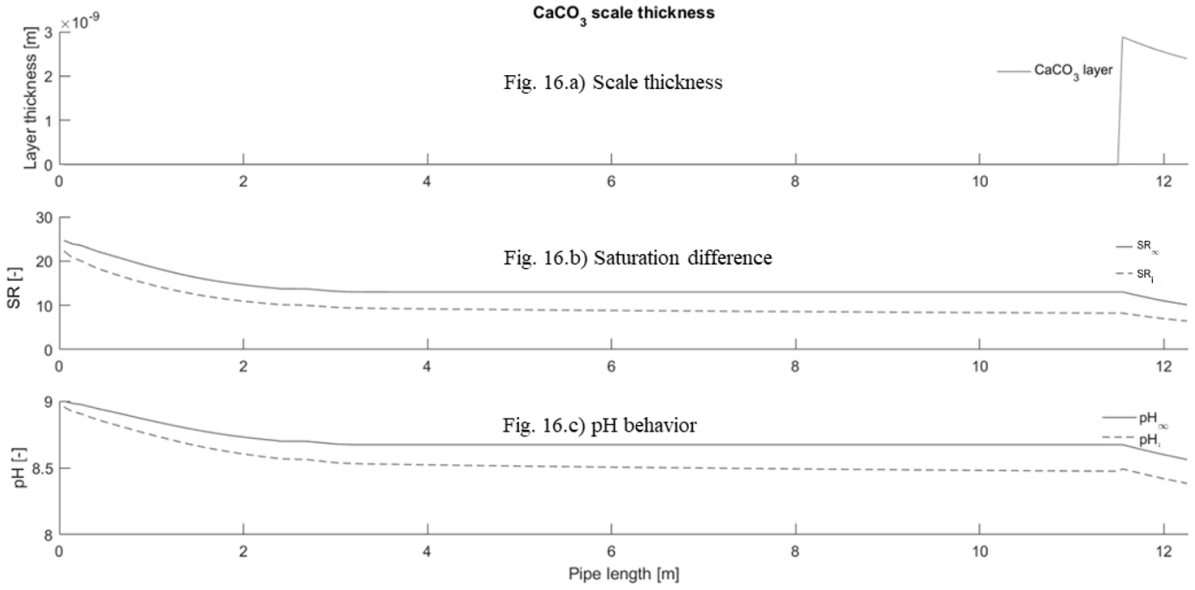

Fig. 16. Kinetic control mechanism behavior (initial DaII = 0.11) Initial bulk solution conditions: pH = 9, $[Ca_T]_\infty$ = $[C_T]_\infty$ = 0.0015 M. Flow conditions: Re=2000 & pipe diameter = 0.1 m. t = 40 minutes.

5.3 Kinetic control mechanism

When the precipitation kinetics is the slower process, calcium carbonate nucleation is shifted downstream and may not form at all in the developing laminar flow region. Within this region, a Damköhler number of 0.11, was selected to display the characteristics of kinetic control. As shown Fig. 16.a, appreciable scaling does not materialize until the flow nears the end of the developing flow due to the slow

precipitation velocity. Since there is no reaction up to this point (~1150 cm), the calcium and carbonate concentrations, as well as the saturation ratio are relatively constant along length of the pipe. Once significant calcium carbonate scaling occurs, the driving force ($SR_\infty - SR_i$) remains almost uniform, but a distinct inflexion point is evident (Figure 16.b); the bulk and interfacial pH values follow a similar tendency. The slight variation of the pH and SR values, near the pipe entrance results from a Damköhler number ($Da_{II} = 0.11$) that is marginally influenced by the mass transfer rate; for smaller Damköhler numbers (when the reaction velocity is yet slower), these values will change even less (however, a smaller Da_{II}, would not show the characteristics of inflexion within the developing flow region). In the case of the kinetics controlling mechanism, the bulk and interfacial saturation ratio profiles, as well as the pH values, decrease much less and in a more linear manner along the pipe length in comparison with the other two cases.

5.4 Comparison of the controlling mechanism behaviors over time

The behaviors shown for the three mechanisms were explained in the previous sections considering a fixed time; in the present section, a comparison is made between the deposit growth characteristics for the three mechanisms at two different times (see Figures 17.a - 17.f). At short times (40 minutes), in two first cases (controlled by mass transfer and mixed control) the behavior is quite similar: the major layer thickness is at the pipe inlet (see Fig 17.a and 17.b, although in the mixed control case, the maximum accumulated deposit was only one third of that corresponding to the mass transfer case. In the kinetic-controlled, case (see Fig. 17.c), the significant scale profiles appear at approximately 1150 cm from the inlet and its thickness is relatively small compared to the other two mechanisms.

The accumulated $CaCO_3$ deposit after an extended period (140 days) are shown in Figures 17.d), 17.e) and 17.f) for the mass transfer, mixed and kinetic controlled mechanisms, respectively. The three figures show growths of the calcium carbonate layer similar behaviors to those at the short time period for each mechanism: in the mass transfer- controlled case, the accumulation is notoriously concentrated at the pipe entrance and when the precipitation velocity is controlling, the deposits are small and appear much further downstream. As was mentioned previously, the main factor that will determine the controlling mechanism is the affinity between the tube material and calcium carbonate deposit.

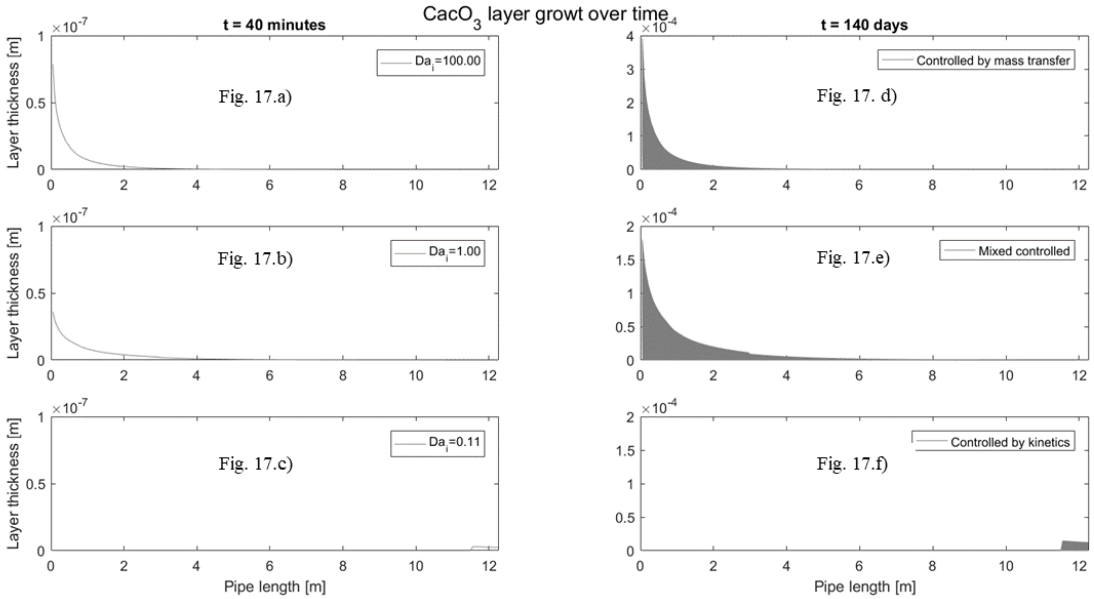

Fig. 17. Growth of the calcium carbonate layer at two different times for the three mechanisms. Initial bulk solution conditions: pH = 9, $[Ca_T]_\infty = [C_T]_\infty = 0.0015$ M. Flow conditions: Re=2000 & pipe diameter = 0.1 m.

Conclusions

The present investigation develops a model for calcium carbonate deposit formation, considering solution equilibria and hydrodynamic phenomena, in developing laminar flow. This model describes the mass transfer of the distinct species from the bulk solution to the pipe wall (deposition surface), coupled with the deposition kinetics. The driving force for both processes are expressed in terms of the local saturation ratios.

In this research, the major contribution is to extend the classical description of chemical equilibria to situations involving complex flow phenomena. The mass transfer rate towards the pipe wall is calculated as a function Reynold number and the distance from the pipe entrance.

Mass-transfer and kinetic-control processes are simulated. In the first scenario, the calcium carbonate layer was concentrated at the pipe inlet, decreasing exponentially; at a distance far from the entrance, the calcium carbonate layer is insignificant. In the second case, the calcium layer appears further from the pipe inlet; once the calcium carbonate layer develops, a relatively uniform deposit was formed over the pipe length. These findings could help to explain the preferential deposition zones observed in the field.

Acknowledgments

The authors are grateful to the Universidad Nacional Autónoma de México (UNAM) for the PhD scholarship granted to the first author.

NOTATION

a	Effective wetted pipe surface area, [-].
A_T	Mass transfer area, [m^2].
Δz	Discretized length section, [m]
$a_{Ca^{2+}}$	Calcium ionic activity, [mol·m^{-3}].
$a_{CO_3^{2-}}$	Carbonic ionic activity, [mol·m^{-3}].
$C_{A,i}$	Interface concentration, [mol·m^{-3}].
$C_{A,\infty}$	Interface concentration, [mol·m^{-3}].
d	Internal diameter of the pipe, [m].
$f_{Ca^{2+}}$	Calcium ionic activity coefficient, [-].
$f_{CO_3^{2-}}$	Carbonate ionic activity coefficient, [-].
$[Ca^{2+}]$	Calcium ion concentration, [mol·m^{-3}].
$[CO_3^{2-}]$	Carbonate ion concentration, [mol·m^{-3}].
SR	Saturation ratio, [-].
SR_∞	Bulk saturation ratio, [-].
SR_i	Interface saturation ratio, [-].
k_m	Mass transfer coefficient, [m·s^{-1}].
k'_m	Mass transfer coefficient for eq. (40), [s^{-1} m^4 mol^{-1}]
K_{sp}	Solubility product constraint, [mol^2·m^{-6}].
k_{m_j}	Local mass transfer coefficient, [m·s^{-1}].
k_c	Reaction rate constant for calcium carbonate scaling, eq. (38), [s^{-1} m^4 mol^{-1}]
k	Temporal discretization, [-].
L_T	Total pipe length, [m].
L_j	Discretized section pipe length, [m].
N_{Ca_T}	Total calcium flux, [mol·s^{-1}·m^{-2}].
N_{C_T}	Total carbonate flux, [mol·s^{-1}·m^{-2}].
N_G	Global flux, [mol·s^{-1}·m^{-2}].
$\dot{n}_{Ca_{T_{trans}}}\big\vert_j$	Moles of total calcium transferred to the pipe wall, [mol·s^{-1}].
$\dot{n}_{C_{T_{trans}}}\big\vert_j$	Moles of total carbonate transferred to the pipe wall, [mol·s^{-1}].
$n_{CaCO_{3_{prod}}}$	Calcium carbonate moles produced, [mol].
$\mathbb{R}_{CaCO_3}$	Precipitation reaction rate at the pipe wall, [mol·s^{-1}·m^{-2}]
Sc	Schmidt number, [-].
Sh	Sherwood number, [-].
Sh_j	Local Sherwood number, [-].
j	Pipe length discretization, [-].
$\mathscr{D}$	Diffusion coefficient, [m^2·s^{-1}].
v^0	Fluid average velocity, [m·s^{-1}].

References

Bailey, B., Crabtree, M., and Tyrie, J. (2000). Water Control. *Oilfield Review 12*(1), 30-51.

Chan, S., and Ghassemi, K. (1991). Analytical modeling of calcium carbonate deposition for laminar falling films and turbulent flow in annuli: Part I -formulation and single-species model. *Journal of Heat Transfer*. 735-740. https://doi.org/10.1115/1.2910625

Chan, S., and Ghassemi, K. (1991). Analytical modeling of calcium carbonate deposition for laminar falling films and turbulent flow in annuli: Part II - multispecies model. *Journal of Heat Transfer*, 741-746. https://doi.org/10.1115/1.2910626

Cussler, E. (2009). *Diffusion: Mass Transfer in Fluid Systems*. 3rd edition. Cambridge University

Press, USA.

Cowan, J., and Weintritt, D. (1976). *Water-Formed Scale Deposits*. Gulf Publishing Company, USA.

Crabtree, M., Eslinger, D., Fletcher, P., Miller, M., Johnson, A. and King, G. (1999). Fighting scale -removal and prevention. *Oilfield Review 11*(3), 30-46.

Epelle, E., and Dimitrios G (2018). A CFD investigation of the effect of particle sphericity on wellbore cleaning efficiency during oil and gas drilling Proceedings of the 28th *European Symposium on Computer Aided Process Engineering*. https://doi.org/10.1016/B978-0-444-64235-6.50024-3

Eroni, V., Neville, A., Kapur, N. and Euvrad. M. (2013). New insight into the relation between bulk precipitation and surface deposition of calcium carbonate mineral scale. *Desalination and Water Treatment 51*, 882-891.

Kammal, M., Hussein, I., Mahmoud, M., Sultan, A., and Mohammed. A. (2018). Oilfield scale formation and chemical removal: A review. *Journal of Petroleum Science and Engineering 171*, 127-139. https://doi.org/10.1016/j.petrol.2018.07.037

Kang, P. S., Hwang, J. Y., and Lim, J. S. (2018). Flow rate effect on wax deposition behavior in single-phase laminar flow. *Journal of Energy Resources Technology 141*(3), 032903. https://ph02.tci-thaijo.org/index.php/MIJEEC

Lapidus, G. (1992). Mathematical modelling of metal leaching in ponporous minerals. *Chemical Engineering Science 47*(8), 1933-1941. https://doi.org/10.1016/0009-2509(92)80311-Y

Lobo-Oehmichen, R. (2007). *Principios de Transferencia de Masa*. Universidad Autónoma Metropolitana, México.

Lake, L., W. (1989). *Enhanced Oil Recovery*. Prentice Hall. USA.

Lévêque, J. (1928). *Annales des Mines*, Memoires, Series 12, 13, 201-299, 305-362, 381-415.

MEDUSA. KTH Royal Institute of Technology. School of Chemical Science and Engineering. https://www.kth.se/en/che/medusa/downloads-1.386254. Accessed June 2017.

Rostron, P. (2018). Critical review of pipeline scale measurement technologies. *MOJ Mining and Metallurgy 1*(1), 22 -35.

Segev, R., Hasson, D. and Semiat, R. (2012). Rigorous modeling of the kinetics of calcium carbonate deposit formation. *AIChE Journal 58*(4), 1222-1229. https://aiche.onlinelibrary.wiley.com/doi/10.1002/aic.12645

Skelland, A. (1974). *Diffusional Mass Transfer*. John Wiley & Sons, Cambridge. USA.

Society of Petroleum Engineers. (2017). Scale Problems in Production. Available at: http://petrowiki.org/Scale_problems_in_production. Accessed: September 2017.

Weichers, S., Sturrock, P., and Marais, G. (1975). Calcium carbonate crystallization kinetics. *Water Research 9*(9), 835-845. https://doi.org/10.1016/0043-1354(75)90143-8

Wolthers, M., Nehrke, G., Gustafsson, J.P., and Van Cappellan, P. (2012). Calcite growth kinetics: Modeling the effect of solution stoichiometry. *Geochimica et Cosmochimica Acta 77*, 121-134. https://doi.org/10.1016/j.gca.2011.11.003

Zhang, P., Zhang, Z., Liu, Y., Kan, T., and Tomson M. (2018). Investigation of the impact of ferrous species on the performance of common oilfield scale inhibitors for mineral scale control. *Journal of Petroleum Science and Engineering 172*, 288-296. https://doi.org/10.1016/j.petrol.2018.09.069

Zhang Y. and Dawe, R. (1997). The kinetics of the calcite precipitation from a high salinity water. *Applied Geochemistry 13*, 177-184. https://doi.org/10.1016/S0883-2927(97)00061-9

Zhang Y, Shaw H, Farquhar R and Dawe, A. (2001). The kinetics of carbonate scaling-application for the prediction of downhole carbonate scaling. *Journal of Petroleoum Science and Engineering 29*, 85-95. https://doi.org/10.1016/S0920-4105(00)00095-4

Zhu, G., Li, H., Li, S., Hou, X., Xu, D., Lin, R. and Tang, Q. (2015). Crystallization behavior and kinetics of calcium carbonate in highly alkaline and supersaturated system. *Journal of Crystal Growth 428*, 16-23. https://doi.org/10.1016/j.jcrysgro.2015.07.009